scientific reports

Check for updates

OPEN

Simulation study of low-level disturbances affecting near surface inversion events in Urumqi

Ren Cai[1], Xian Yang[2] & Keming Zhao[3]✉

With accelerated urbanization, temperature inversion phenomena are becoming more prominent in urban atmospheric environments, playing a very important role in air quality and public health. Despite the widespread literature on the formation and longevity of inversions, little is understood about the measures to mitigate them. Filling this knowledge gap, this work examines the impact of low-level artificial perturbations on near-surface inversions through the use of numerical modeling. The case is selected from an inversion event in Urumqi at 08:00 on 19 January 2023. Numerical simulations were done using the Fluent fluid dynamics model and the Advanced Regional Prediction System (ARPS) model. The results indicate that the application of low-level perturbations can destabilize inversion layers, cause vertical mixing, and promote atmospheric instability. Comparative experiments with the two models confirm that external perturbations disrupt stability stratification, enabling exchange and dispersion of air and pollutants. The simulations also indicate that increased inflow wind speeds facilitate atmospheric turbulence, leading to increased instability and improved air quality. Specifically, the thickness of the inversion layer decreased by approximately 40% after two hours of disturbance, and after three hours the inversion was practically eliminated. The Fluent model indicates localized flow field changes, while the ARPS model simulates the large-scale atmospheric response. The two-model approach provides an integrated picture of the processes for the breakdown of the inversion layer. The results provide new insight into the control of urban air pollution, with the implication that certain artificial disturbances can be employed as an effective method for the mitigation of temperature inversions in highly polluted cities.

Keywords Numerical simulation, Turbulence model, Fluent, ARPS, Inversion disruption, Intensity variation

Maintaining the environment healthy is crucial for the public because it directly affects health, ecosystem balance, and the general quality of life[1–3]. Air and atmospheric conditions play a crucial role in deciding the quality of the air[4]. The deterioration of air quality is closely related to meteorological conditions, particularly atmospheric temperature inversions, which stabilize the atmosphere, slow down air circulation, and thereby inhibit the horizontal and vertical dispersion of pollutants[5]. Additionally, the thickness of the mixed layer is a crucial factor in the dilution and dispersion of air pollutants. When the mixed layer is thin, pollutants are less likely to disperse vertically, leading to aggravated pollution levels[6,7]. During near-surface inversions, wind speeds are generally low, further hindering pollutant dispersion. The stronger, thicker, and longer-lasting the inversion layer, the more severe the pollution tends to be[8].

Urumqi, located in central Xinjiang and surrounded by mountains on three sides, including the northern slopes of the Tianshan Mountains, is particularly prone to severe inversion-related weather due to its geographical location. This issue becomes especially pronounced in winter when solar radiation weakens. Under valley winds, the layer of inversion becomes more intense[9–11]. During the night, the valley winds typically blow downslope and carry cold air to the lower regions of the city. It intensifies the cooling at the surface and makes the layer of inversion more intense by maintaining the air mass cooler at the surface and warmer air above it. Additionally, the valley wind circulation can limit the horizontal dispersion of the pollutant by confining the air mass in the valley structure, contributing to air pollution. Analyses of the vertical distribution of atmospheric pollutants show that aerosol concentrations are highest within 500 m of the ground. Studies indicate that in winter, the thickness of Urumqi's surface inversion layer increases significantly, reaching its maximum in January, with values of 486 m at 08:00 and 510 m at 20:00[12,13]. The maximum thickness of elevated inversions occurs in December, with 430 m

[1]Urumqi Meteorological Bureau, Urumqi, Xinjiang, China. [2]Meteorological Service Center of Xinjiang Uygur Autonomous Region, Urumqi, Xinjiang, China. [3]Meteorological Observatory of Xinjiang Uygur Autonomous Region, Urumqi, Xinjiang, China. ✉email: zhaokeming_1983@163.com

at 08:00 and 380 m at 20:00, and the highest inversion altitude reaching 566 m[14,15]. The Report on Atmospheric Pollution Countermeasures in Autumn and Winter for the Urban Agglomeration on the Northern Slopes of the Tianshan Mountains highlights that periods of severe pollution often occur during conditions of high humidity and low wind speeds. When the boundary layer height is below 0.5 km, the increased water vapor content facilitates the local accumulation of pollutants.

Currently, research on the inhibitory effects of inversion layers on the dilution and dispersion of air pollutants in this region is relatively comprehensive[16]. However, studies on how to weaken or eliminate inversions remain insufficient. The majority of efforts in China, including Urumqi, have been on techniques like cloud-seeding and artificial precipitation, which try to modify the distribution of temperature and humidity in the atmosphere in order to reduce or eliminate inversion layers[17,18]. Although these methods claimed effectiveness under certain conditions, they are highly dependent on specific weather scenarios. What's more, because of inadequate theoretical support and numerical simulation results, the scientific guidance for weakening or eliminating an inversion layer artificially is often lacking, leading to costly strategies with far-from-optimal outcomes.

This study addresses this knowledge gap by examining the impact of controlled artificial perturbations on dissipation in near-surface inversion layers. We utilize both the Fluent computational fluid dynamics (CFD) model and the Advanced Regional Prediction System (ARPS) model to investigate the impact of controlled perturbations on the stability and dissipation of inversions. We compare the two models to analyze the efficiency of artificial perturbations in enhancing vertical mixing and reducing the intensity of inversions. Results provide new insight into potential mitigation strategies for air pollution in cities frequently afflicted by temperature inversions.

Simulations play an indispensable role in the investigation of complex systems to obtain insight into the interaction at different space and time scales[19]. Numerical simulations are particularly crucial for the investigation of environmental and fluid dynamics problems because they can describe the vast array of physical processes that control such systems[20,21]. Several modeling approaches are required to describe the vast array of physical processes that control environmental and fluid dynamics[22–25]. A three-dimensional modeling framework is required to describe these interactions and their effects on the system effectively[26]. This research makes use of the coupled modeling method with Fluent and the Advanced Regional Prediction System (ARPS) to couple high-resolution computational fluid dynamics with large-scale atmospheric modeling. Fluent, which is computational fluid dynamics (CFD) software, has been used widely in meteorology to model urban wind fields and pollutant dispersion because it can operate at high spatial resolution. It offers several turbulence models for the examination of airflow characteristics, making it applicable to the investigation of the disturbance of the inversion layer. It is, however, lacking in the inclusion of large-scale atmospheric processes because Fluent is used mainly for industrial fluid dynamics. On the other hand, the Advanced Regional Prediction System (ARPS) model, which was created to model mesoscale and microscale weather, gives a wider atmospheric view, including storm and boundary layer dynamics. This research combines the two models with the view to taking advantage of the strengths of the two methods to investigate the efficiency of artificial disturbance in breaking the near-surface inversions.

On the other hand, the Advanced Regional Prediction System (ARPS), developed by the Center for Analysis and Prediction of Storms at the University of Oklahoma, is a non-hydrostatic atmospheric numerical prediction model with the capability of full-scale storm prediction. ARPS integrates real-time data assimilation systems, forward integration forecast models, and post-processing modules, making it suitable for high-resolution numerical simulations at the meter scale. The model has been widely applied in fields such as hailstorms, thunderstorms, heavy rainfall, and atmospheric pollution. By incorporating simplified surface parameterization schemes, the simulation capabilities of ARPS in urban boundary layers have been significantly enhanced[27]. Whereas ARPS addresses large-scale atmospheric responses to cities, it does not explicitly address small-scale details. It addresses them indirectly by employing parameterizations for the urban canopy to make an estimation for the overall impact of buildings on airflow and turbulence. This deficiency necessitates the coupling with Fluent, which provides finer-resolution simulation to address fine-scale city airflow and mixing processes. For the context of this research, the introduced low-level perturbations interact with such flow structures by altering the pressure gradients and enhancing the mixing due to the turbulence. Wake vortices and canyon recirculations modulate the propagation of artificial disturbance in the urban boundary layer, modulating the dissipation of the inversion layer. Vertical mixing is augmented by the interaction with such vortices and the external disturbance, which enhances the pollutant dispersion and reduces the stability of the inversion. Another study used aircraft load factor equations to do a flight numerical simulation after simulating the wind field needed for airflow over mountainous terrain using ARPS. According to the study, airplanes experienced clear-air turbulence as a result of the wind shear critical layer fragmenting and the gravity waves created by airflow passing over the mountains creating strong turbulence in the troposphere. Aircraft takeoff and landing were also impacted by low-altitude turbulence, leeward rotor circulations, and strong downslope winds that developed on the leeward side of the mountains. In order to improve turbulence prediction and flight weather safety, this study uncovered the physical process causing aircraft turbulence when flying in leeward atmospheric turbulence. However, there is still a lack of research on how these models simulate and reproduce flow field disturbances or inversion layers. Whereas Fluent is better suited for industrial fluid dynamics analysis, ARPS concentrates on simulating mesoscale and microscale weather systems. Each model is able to succeed in its own field because of this scale disparity. While Fluent concentrates on fluid flow and heat and mass transfer, ARPS prioritizes atmospheric dynamics, thermodynamics, and microphysical processes when it comes to simulating physical processes. Urban surface forcing and boundary layer interchange are involved in lower-layer disturbances, and the process of inversion layer disruption cannot be well captured by Fluent or ARPS alone. Consequently, in order to do comparative analysis and study the mechanisms underlying inversion layer evolution, combined simulations utilizing both models are required. Application of both models in a combined way allows the performance of

cross-scale simulations-from micro-scale fluid dynamics to macro-scale atmospheric environments-and fills the gaps left by using any one model in simulating complex atmospheric phenomena. Highly precise fluid simulation by Fluent captures the subtle flow characteristics under those complicated meteorological conditions, such as inversion layers, while ARPS provides its wider atmospheric background and boundary conditions. Due to the integration of the two models, the results of the simulation are closer to realistic situations, hence increasing the accuracy and reliability for these simulations.

This work investigates an inversion phenomenon in Urumqi with the occurrence of strong stability, light surface winds, and thick layering—conditions characteristic for the winter period, hence typical for the common winter inversions in the region. It also examines the impact of low-level artificial perturbations on near-surface inversions through the application of numerical modeling. This research will be based on both the Fluent and ARPS models in an attempt to compare the two models with the purpose of validating each other's simulation results and finding out how consistent these two models can be. It'll seek, through dual simulations, to ascertain whether artificial disturbances can effectively knock down the inversion layer and enhance atmospheric instability to support regional air pollution control.

Data and methods

The Fluent model uses real-time radiosonde data from the Urumqi Meteorological Station at 08:00 on January 19, 2023, as the initial field, aiming to closely replicate actual conditions in the simulation experiment. Figure 1 displays the radiosonde data from the Urumqi National Meteorological Reference Station at 08:00 on January 19, 2023, with the blue line representing the temperature profile. The near-surface air temperature was − 20.4 °C (at an elevation of 936 m), and it increased to − 18.2 °C at a height of 28 m, then to − 12.9 °C at 163 m, and further rose to − 9.5 °C at 293 m. The highest temperature of the inversion layer occurred at 490 m, reaching − 7.8 °C.

Before conducting the simulation, it is necessary to perform a sensitivity analysis on key parameters such as physical properties and boundary conditions. After multiple simulations, the optimal parameter combination was determined to refine the simulation setup and improve the accuracy of the results. Therefore, selecting appropriate simulation time, region, and parameters, along with conducting sensitivity analysis, is a crucial step in designing Fluent simulation experiments. For the sake of precision, this process included the systematic adjustment of simulation parameters in line with observed atmospheric conditions, literature research, and expert recommendations. Sensitivity tests were performed to experiment with the influence of different turbulence models, grid resolutions, and inflow wind conditions on simulation stability and precision. Meanwhile, the ARPS model utilizes the NCEP GFS forecast field from the United States to generate background fields and boundary conditions.

In this study, the Realizable $\kappa - \varepsilon$ turbulence model was employed, which is a two-equation turbulence model specifically designed for simulating turbulent phenomena in computational fluid dynamics (CFD). The Realizable $\kappa - \varepsilon$model improves upon the standard $\kappa - \varepsilon$ model by considering the effects of shear and rotational flows while maintaining a structure similar to the traditional $\kappa - \varepsilon$ model. This equation is suitable for various complex turbulent flows. The transport equations are as follows:

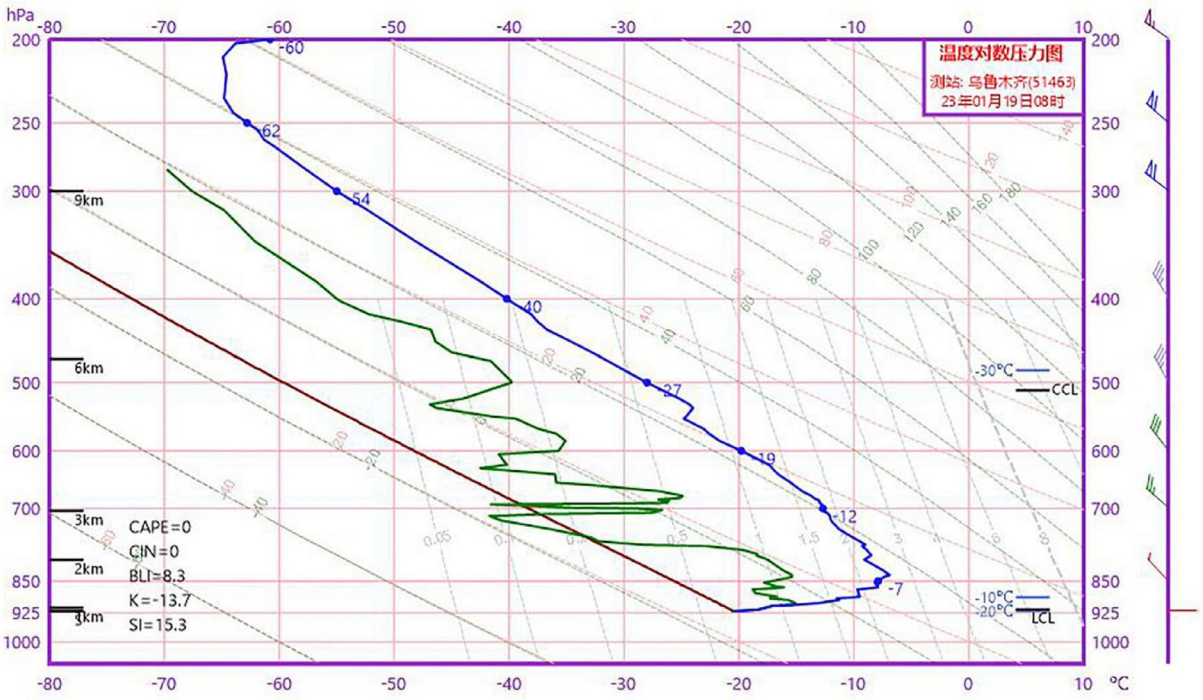

Fig. 1. Temperature variation with height and pressure (the blue line represents the temperature profile).

Equation κ:

$$\frac{\partial}{\partial t}(\rho k)+\frac{\partial}{\partial x_j}(\rho u_j k)=\frac{\partial}{\partial x_j}\left[\left(\mu+\frac{\mu t}{\sigma k}\right)\right]-P_{ij-j}-G_k+b_k \tag{1}$$

Equation ε:

$$\frac{\partial}{\partial t}(\rho\varepsilon)+\frac{\partial}{\partial x_j}(\rho u_j\varepsilon)=\frac{\partial}{\partial x_j}\left[\left(\mu+\frac{\mu t}{\sigma\varepsilon}\right)\frac{\partial\varepsilon}{\partial x_j}\right]+C_{1\varepsilon}\frac{\varepsilon}{k}-C_{2\varepsilon}\frac{\rho^{\frac{1}{2}}}{\sigma\varepsilon}\left(\frac{\varepsilon}{k}\right)^{\frac{3}{2}}+C_{3\varepsilon}\rho^{-1}/3 \tag{2}$$

In the Realizable k–ε turbulence model, the variables in the transport equations represent different physical properties of the turbulent flow. P is the air density, k is the turbulent kinetic energy, and ε is the turbulence dissipation rate. u_j represents velocity components in different directions, while P_k is the production term due to mean velocity gradients, and P_b accounts for the generation term due to buoyancy. The constants C_1 and C_2 are model coefficients, ν denotes the kinematic viscosity, and S represents the strain rate effects. Compared to the standard k–ε model, the Realizable k-ε model accounts for more physical effects, making it more reliable and accurate across a wider range of flow situations. It has been widely applied in fields such as fluid mechanics and environmental fluid dynamics to address complex turbulent problems.

Where P_{ij-j}represents the production term due to mean velocity gradients, $G_k$represents the generation term due to buoyancy, and B_k represents the strain rate generated by production, which indicates the strain rate due to the production effect. These terms vary depending on the specific flow conditions and need to be determined by solving the transport equations. Compared to the standard $\kappa-\varepsilon$ model, the Realizable $\kappa-\varepsilon$ model accounts for more physical effects, making it more reliable and accurate across a wider range of flow situations. It has been widely applied in fields such as fluid mechanics and environmental fluid dynamics to address complex turbulent problems.

ARPS Model Governing Equations:

$$x_1=x_0+r\cos(\alpha),y_1=y_0+r\sin(\alpha) \tag{3}$$

$$u(x_1,y_1)=u_0(x_1,y_1)-\mathbf{v}\sin[180+(90-\alpha)] \tag{4}$$

$$v(x_1,y_1)=v_0(x_1,y_1)-\mathbf{v}\cos[180+(90-\alpha)] \tag{5}$$

.

In this system, the coordinates of the wind tower are x_0, y_0, (x_i,y_i), $i=1...5$, and the wind turbine coordinates are

In this system, the coordinates of the wind tower arex_0, y_0, and (x_i,y_i), where i =1…5, represent the coordinates of the wind turbines. *r* is the radial distance from the wind turbine to the center of the wind tower, **v**is the wind speed at the turbine, and $\alpha$is the rotational angle.

Fluent model simulation setup

To generate the three-dimensional data required for Fluent simulations, second-by-second radiosonde data from the Urumqi National Reference Station was utilized to create a 3D grid that includes temperature, humidity, air pressure, and wind speed information. The Fluent simulation domain, covering a 1 km × 1 km area, is positioned near the center of the ARPS simulation domain, corresponding to an urban region within Urumqi. The simulation domain was set as a cuboid with dimensions of 1000 m in length, 1000 m in width, and 600 m in height. The grid resolution was defined as 100 × 100 × 60, with a spatial resolution of 10 m×10 m×10 m. A three-dimensional model was employed in this study, where the grid was divided into two parts: an external fixed grid region and an internal rotating grid region, yielding a total grid count of approximately 12 million cells. The simulation used the standard Realizable $\kappa-\varepsilon$ turbulence model. For the wind column motion, the sliding mesh method was applied. The ground was set as a no-slip fixed boundary, while the pressure outlet boundary condition at the top was defined by a user-defined function (UDF). Similarly, the temperature at the top was also set using a UDF. The side pressure and temperature variations were configured through UDF files, which allowed for defining the variation of pressure and temperature with height. The internal grid region was set to rotate at a speed of 0.75 RPM. The simulation time step was 0.01 s, with the possibility of increasing the time step after the simulation stabilized. All simulations were performed using second-order accuracy, covering turbulence parameters and the energy equation. Although the individual buildings were not explicitly solved here, they would have the potential to greatly influence the surface turbulence, alter the wind patterns, and modify the disturbance propagation. Building-resolving simulations in the future can provide more insight into such effects.

ARPS model simulation setup

The center coordinates of the ARPS simulation domain were set to (43.783° N, 87.65° E), using Lambert map projection with a resolution of 500 m. The horizontal grid consisted of 363 × 363 points, and the vertical grid had 53 layers with a vertical resolution of 500 m. The background field and lateral boundary conditions were generated from the NCEP GFS (Global Forecast System) forecast field. The initial model time was set to 08:00 on January 19, 2023 (Beijing time), with an integration time step of 0.8 s and a total integration period of 24 h. The terrain and land surface data had a resolution of 30 arc seconds (approximately 900 m). The physical schemes employed included the Lin ice-phase cloud microphysics scheme, atmospheric radiation transfer parameterization, and the 1.5-order TKE turbulence mixing parameterization scheme[28]. To generate the three-dimensional data required

for the ARPS model, wind fields, temperature fields, equivalent potential temperature, vertical velocity, vertical temperature gradient, and the radial component of vertical circulation were extracted and calculated from the NCEP GFS data[29]. The ARPS model employed a 17 × 17 km square grid at the surface, and the simulation height extended up to 3 km.

Model validation

For the verification of the reliability of the simulation result, the simulated temperature and wind field profiles were validated against the observed radiosonde records at the Urumqi National Meteorological Reference Station. Sensitivity tests were also conducted to test the stability of the model for varying disturbance conditions. The result demonstrated excellent agreement between the simulation and observation, confirming the reliability of the numerical method in simulating the properties of inversions and the disturbance effects.

Simulation results analysis

Fluent model results analysis

In the Fluent model, temperature, air pressure, and humidity from the radiosonde data were introduced as the initial field. As shown in Fig. 2, the inversion layer in Urumqi is not horizontally uniform across the region, and the thickness of the inversion layer varies in different areas. Overall, the trend of temperature change with height remains consistent. In this sensitivity experiment's simulated atmosphere, the temperature lapse rate is relatively high, the air motion remains steady, and the atmospheric layer is overall stable. The vertical stability of the atmosphere plays a crucial role in the dispersion and transport of air pollutants within the atmospheric layer.

The presence of the inversion layer leads to cold air near the surface being trapped under warmer air aloft, forming a stable stratified structure. However, when a disturbance is introduced at the base of the inversion layer, this stable structure begins to break down. The disturbance causes an exchange between the surface cold air and the warmer air above, leading to atmospheric instability. This increase in instability promotes the diffusion of vertical motion, which also enhances horizontal dispersion, as illustrated in Fig. 3a.Under the framework of the Realizable $\kappa - \varepsilon$ turbulence model, the effect of this disturbance on the stable atmospheric structure can be explained using the transport equations for turbulent kinetic energy κ and turbulent dissipation rate ε. When the disturbance occurs, the turbulent kinetic energy κ starts to increase, indicating an enhancement of the turbulent motion within the fluid. Simultaneously, the dissipation rate ε changes, reflecting the dissipation of turbulent energy over time and space. During the disturbance of the inversion layer, the increase in turbulent motion allows for more effective mixing between the cold surface air and the warmer air aloft. This mixing process not only alters the temperature distribution in the atmosphere but also affects the density and pressure distributions. As the disturbance progresses, the structure of the inversion layer gradually breaks down, as shown in Fig. 3b. At this point, the warmer air above funnels downward, mixing intensely with the colder air below. In the Realizable $\kappa - \varepsilon$ model, the turbulent viscosity $\mu_t$is related to both $\kappa$and ε, reflecting the impact of turbulence on fluid flow. During the disturbance of the inversion layer, the increase in turbulent viscosity enhances the frequency and

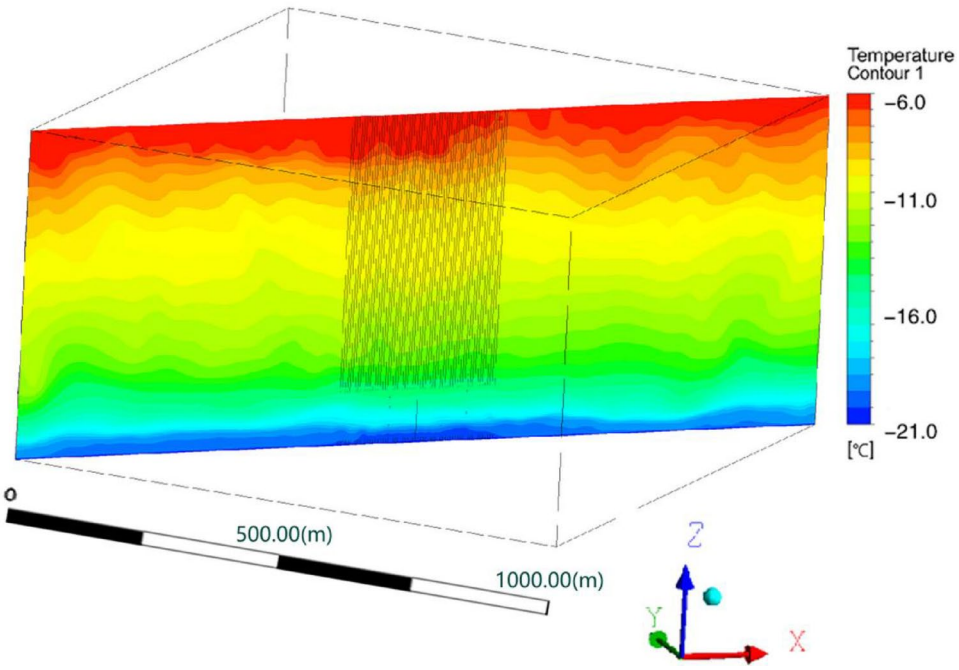

Fig. 2. Temperature variation with height. The vertical axis represents altitude (m), and the blue line shows the temperature profile. The sky-blue marker indicates the radiosonde measurement point, while the shaded section highlights the core of the inversion layer.

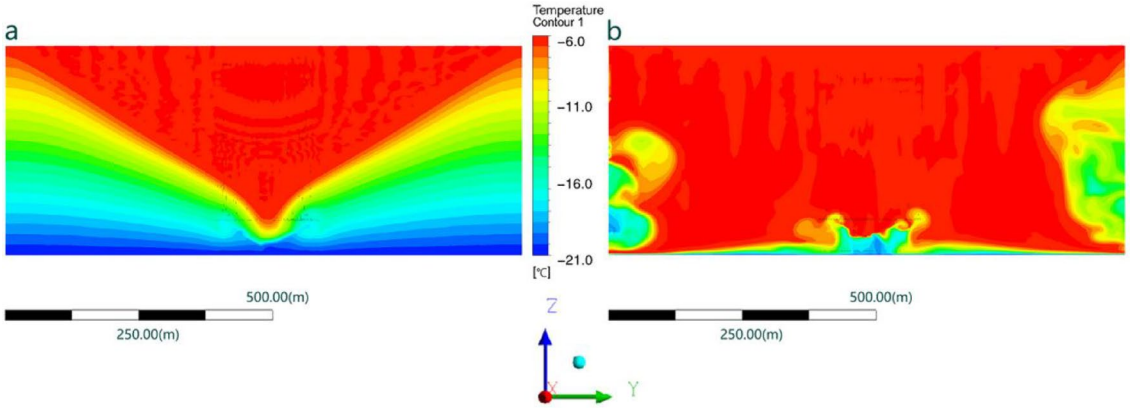

Fig. 3. Effect after two hours of disturbance (**a**), effect after three hours of disturbance (**b**). The vertical axis represents altitude (m). Shaded areas indicate regions of intensified turbulence, leading to inversion weakening.

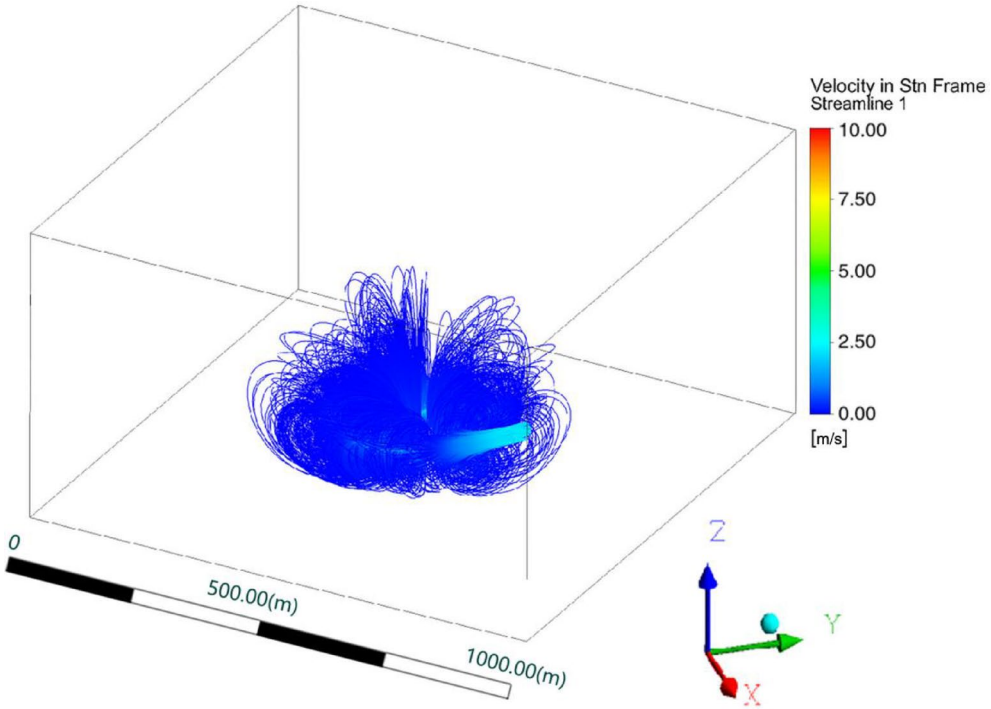

Fig. 4. Velocity streamlines after 2 h of disturbance. The vertical axis represents altitude (m). Thicker streamlines indicate stronger velocity fields, illustrating the impact of artificial disturbances.

efficiency of momentum exchange between fluid particles. This momentum exchange facilitates the diffusion of vertical flows and intensifies horizontal dispersion, further accelerating the breakdown of the inversion layer.

Furthermore, the model constants (such as $C_{1\varepsilon}$, $C_{2\varepsilon}$and$C_{3\varepsilon}$) and the turbulent Prandtl numbers (such as σ_κ, σ_ε) in the Realizable $\kappa-\varepsilon$ model are critical to the accuracy of the simulation results. These parameters must be optimized based on experimental data and theoretical analysis to ensure that the model accurately reflects the physical phenomena in the actual flow process.

The disturbance at the base of the inversion layer causes cold air near the surface to diffuse outward, which triggers a compensating downward flow of warm air from the upper atmosphere. A low-pressure zone forms at the wind turbine platform, allowing warm air from above to flow into this low-pressure area, while the surrounding high-pressure zones are unable to continue expanding outward. This results in an upward motion, forming small-scale circulations. As shown in Fig. 4, the velocity streamlines from the Fluent simulation illustrate both vertical and horizontal velocity components two hours after the disturbance. Analyzing the streamlines reveals that the disturbed flow aligns with the initial sensitivity experiment design, where the fluid streamlines change after the disturbance. The streamline results indicate that the application of external pressure causes the air to first diffuse outward, then move upward, and eventually converge toward the center. By artificially increasing the

disturbance, larger vortices are formed, which leads to the breakdown of the stable inversion layer. This process, examined through sensitivity experiments involving the breakdown of the inversion, further reveals the patterns and evolution of the disturbed streamlines.

ARPS model results analysis

The forecast field data from the NCEP GFS (Global Forecast System), released at 08:00, was used as the initial condition for the ARPS model. As shown in Fig. 5a, a significant inversion phenomenon was observed over Urumqi, forming a "thermal bubble" that covers the urban area. The inversion layer can be viewed as a "thermal bubble" floating on top of a stable atmosphere, with its highest temperature point located approximately 300 to 500 m above the city. Above 600 m, the atmosphere becomes unstably stratified. For computational efficiency, the top height of the Fluent model's three-dimensional simulation was set to 600 m, while the ARPS model's top was set to 3 km. A clear inversion layer exists above the city, while other regions exhibit unstable stratified air. The inversion region extends 12 km from north to south, with a height ranging from the ground to 600 m. The airflow primarily consists of downslope winds, and no significant updrafts or downdrafts were observed, as shown in Fig. 5b. The method used to introduce ground-level disturbances in the ARPS model is identical to that in the Fluent model, and sensitivity tests were conducted to explore the feasibility of introducing wind disturbances in Urumqi to break the inversion layer and mitigate pollution.

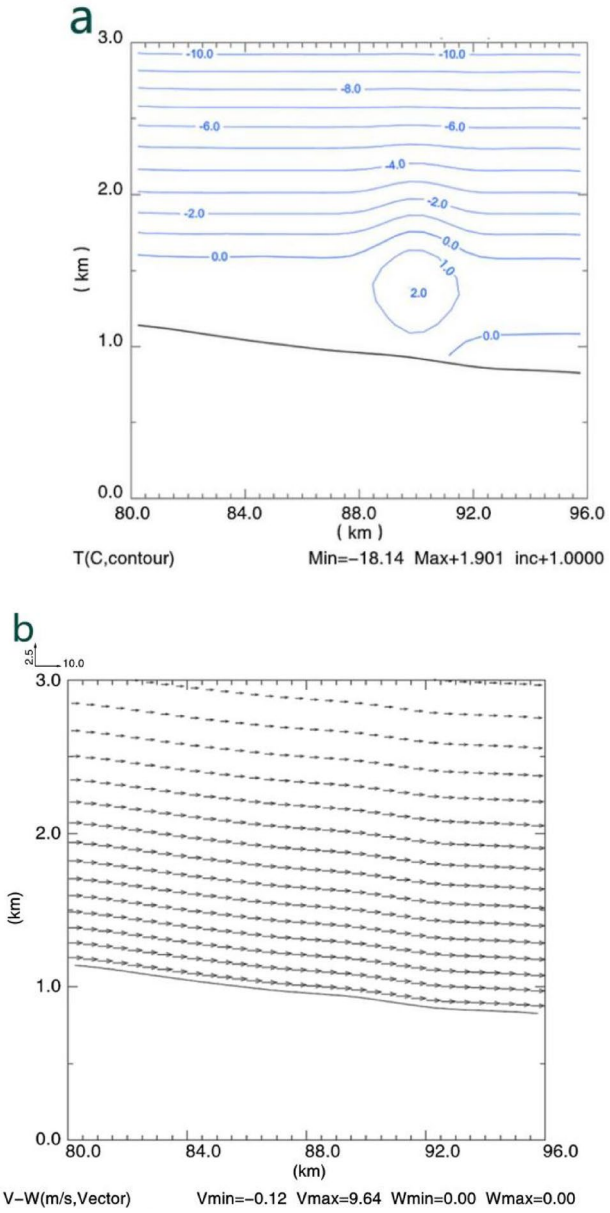

Fig. 5. Meridional-vertical distribution of the initial temperature (**a**) and meridional-vertical circulation at the initial time (**b**).

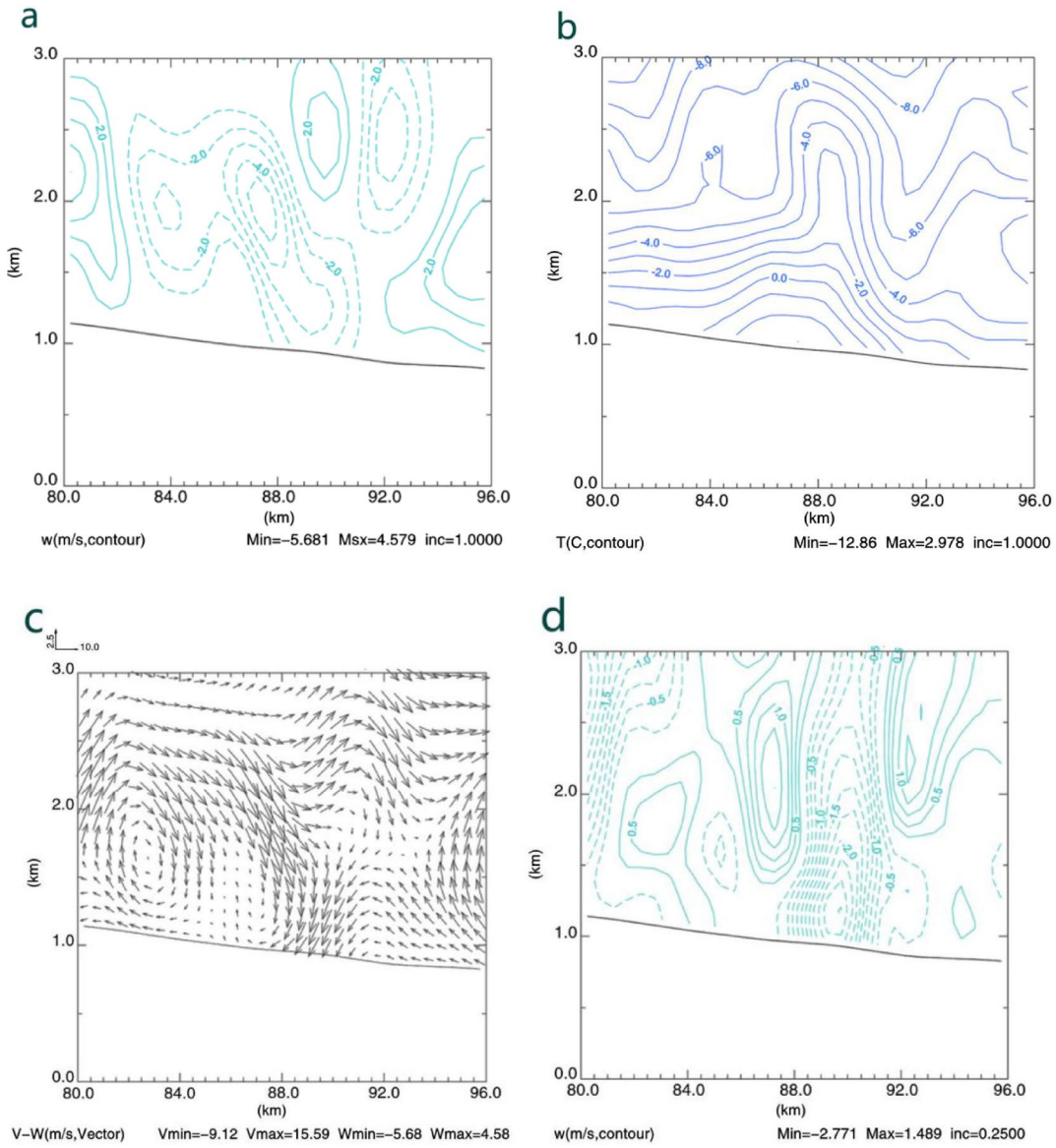

Fig. 6. shows the meridional-vertical distribution of vertical velocity after 2 h of integration (**a**), the meridional-vertical distribution of temperature after 2 h of integration (**b**), the meridional-vertical distribution of vertical velocity after 2 h of integration (**c**), the meridional-vertical distribution of temperature after 3 h of integration (**d**), the meridional-vertical distribution of temperature after 3 h of integration (**e**), and the meridional-vertical distribution of vertical velocity after 3 h of integration (**f**).

After introducing the disturbance at the lower level, observations over a two-hour period revealed the distribution of vertical velocity in the meridional and vertical directions, as shown in Fig. 6a. A significant downdraft appeared above the disturbance area, with a downward velocity of − 3 m/s at around 400 m above the disturbance center. A downdraft was also observed on the left side of the disturbance, with velocities of -4 m/s between the altitudes of 1000 m and 500 m, extending 5 to 6 km horizontally. The maximum downdraft velocity reached 5.68 m/s. Additionally, on the right side of the disturbance, at heights of 2000 m to 800 m and a distance of 5 to 6 km, a downdraft of -3 m/s was observed, indicating that the range of airflow exchange caused by the disturbance exceeded expectations. This phenomenon is consistent with the Fluent simulation results, and the range of airflow exchange significantly expanded, with upper-level warm air moving downward. After three hours of observation, Fig. 6d shows that the maximum downdraft above the disturbance decreased to − 2.77 m/s, and the downdraft had almost reached the surface. This was accompanied by noticeable updrafts on both sides, with vertical velocities exceeding 1 m/s, forming the anticipated small-scale circulations. These results are consistent with the Fluent simulations, indicating a significant enhancement in the exchange of air between the upper and lower layers.

The temperature distribution in the meridional and vertical directions after 2 h of disturbance (see Fig. 6b) shows that the inversion phenomenon had significantly weakened, and the stability of the stratification had

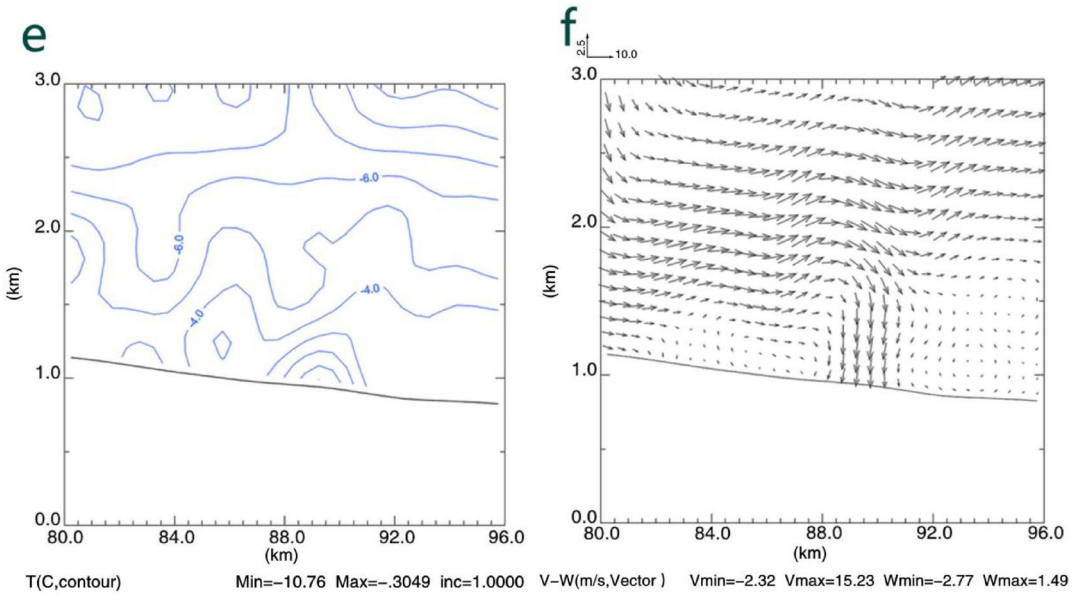

Fig. 6. (continued)

decreased. Compared to the initial temperature distribution in Fig. 5a, the inversion layer was nearly destroyed, and the vertical velocity distribution was consistent with the temperature distribution. After three hours, Fig. 6e shows that the inversion had almost completely disappeared, and the instability of the stratification increased. Compared to the temperature distribution in Fig. 6b, the inversion layer was further destroyed, with the temperature and vertical velocity distributions remaining consistent. In the ARPS model, the mass conservation equation (continuity equation) decomposes the wind velocity vector v into two components, u and v. By calculating these components at different angles, the variations in various physical quantities were derived.

After 2 h of disturbance, the meridional-vertical circulation distribution in Fig. 6c shows a clear, strong downdraft within the disturbed region, accompanied by a significant updraft on the left side. Compared to the initial meridional-vertical circulation distribution (Fig. 5b), significant changes occurred, and the region affected by the simulated disturbance was much larger than that in the Fluent simulation. After 3 h, Fig. 6f shows the formation of a clear downdraft in the disturbed region, with a maximum downdraft velocity of 2.77 m/s. Clear updrafts were also observed on both sides, forming another small-scale circulation. Compared to the initial meridional-vertical circulation distribution (Fig. 6b), there are considerable differences.

Conclusion

This study simulates the breakdown of the inversion layer by applying disturbances at its base, aiming to provide scientific evidence for artificially mitigating inversions and reducing air pollution. The main conclusions are as follows:

1. Disturbances at the base of the inversion layer promote the exchange between the cold air near the surface and the warm air above. Both the Fluent and ARPS model results show that the alternation of cold and warm air enhances atmospheric instability. The vertical diffusion of air flow promotes horizontal diffusion, with the cold surface air spreading outward and the warm air aloft sinking. The intensity and thickness of the inversion layer gradually decrease and are ultimately destroyed. As surface air heats up, atmospheric instability increases, allowing for free exchange between the upper and lower layers. In the Fluent model, the disturbance influences an area with a diameter exceeding 1 km.
2. Setting an inflow point at the center of the grid, with outflow points around it, combined with dynamic disturbances, effectively enhances the diffusion of turbulent energy. If the inflow wind speed is assumed to increase, the transport capacity of the wind field would also strengthen, intensifying turbulence in the atmosphere and further increasing atmospheric instability. The airflow fields obtained from numerical simulations provide a useful approach for air pollution control.
3. The combined simulation using Fluent and ARPS models provides a more comprehensive understanding of the inversion layer breakdown process, offering new insights into the physical processes within the atmospheric boundary layer. This joint simulation approach not only helps address specific atmospheric environmental issues but also advances fundamental research in atmospheric science. The Fluent $\kappa - \varepsilon$ turbulence model and ARPS model used in this study did not consider favorable factors such as solar radiation and valley winds. If these factors were included, the simulation outcomes and the extent of the affected area might be more accurate. As urban development and population growth continue, relying solely on energy conservation and emission reduction may not achieve the balance between air pollution control and rapid economic growth.

4. Both the Fluent and ARPS models effectively demonstrate the role of lower-level disturbances in breaking the inversion layer. The initial field in the Fluent model was derived from radiosonde data, while the ARPS model used NCEP GFS (Global Forecast System) 00-hour forecast data for the initial field. The analysis of the simulation results indicates that dual simulations confirm that introducing artificial disturbances can effectively destroy the inversion phenomenon and enhance atmospheric instability.

These findings suggest that artificial perturbations can be used effectively to suppress or annihilate temperature inversions in cities with severe air pollution. Compared to traditional methods like cloud-seeding and artificial precipitation, which are greatly reliant on favorable meteorology, the imposition of mechanical turbulence provides more reliable and manipulatable means to suppress the influence of inversions. Additionally, the findings here add to the overall understanding of the dynamics of the atmosphere in cities and the role played by mechanical mixing to improve the air quality.

Limitations and Future Outlook: This study employed independent simulations of two models. In the future, coupled simulations will be necessary to more comprehensively reproduce the interaction between lower-level disturbances and the destruction of inversion layers. In particular, future research should focus on analyzing the depth and extent of inversion breakdown after a certain period of disturbance, especially at the urban scale. Given that urban scales typically range from tens of kilometers, it is essential to explore the effects of the intensity and number of local disturbances on improving pollution dispersion at the urban scale.

Data availability

All data generated or analysed during this study are included in this published article.

Received: 8 January 2025; Accepted: 30 May 2025
Published online: 01 July 2025

References

1. Gao, E. et al. Spatio-temporal evolution monitoring and analysis of tidal flats in Beibu Gulf from 1987 to 2021 using multi-source remote sensing. *IEEE J. Sel. Top. Appl. Earth Observations Remote Sens.* (2024).
2. Huang, B. Q. & Li, X. M. Wave attenuation by sea ice in the arctic marginal ice zone observed by spaceborne SAR. *Geophys. Res. Lett.* **50**(21), e2023GL105059 (2023).
3. Zhao, Y. et al. Understanding the weakening patterns of inner Tibetan plateau vortices. *Environ. Res. Lett.* **19** (6), 064076 (2024).
4. Zhao, Y. et al. Remote influence of Southern Tibetan plateau heating on North Pacific atmospheric rivers. *J. Clim.* **38** (1), 101–116 (2025).
5. Li, Z. et al. Aerosol and boundary-layer interactions and impact on air quality. *Natl. Sci. Rev.* **4** (6), 810–833 (2017).
6. Yongqing, H., Yucheng, Z. & Shuqing, F. Temperature inversion in Xining city: characteristics and correlation with air pollutant concentrations. *J. Glaciol. Geocryol.* **36** (3), 608–613 (2014).
7. Bai, Y. et al. Analysis of meteorological conditions and diurnal variation characteristics of PM2. 5 heavy pollution episodes in the winter of 2015 in Hubei Province. *Acta Meteorol. Sin.* **76** (5), 803–815 (2018).
8. Liu, S. et al. Numerical simulation for the coupling effect of local atmospheric circulations over the area of beijing, Tianjin and Hebei Province. *Sci. China Ser. D Earth Sci.* **52**, 382–392 (2009).
9. Zhenjie, L. et al. Characteristics of atmospheric mixing layer height and atmospheric stability in Urumqi region and their relationship with the atmospheric pollution. *Arid Land. Geogr.* **42** (3), 478–491 (2019).
10. Zilong, L. & Dai Bin, C. Z. Concentration characteristics and potential source of atmospheric pollutants: A case study in Urumqi. *Arid Zone Res.* **38** (2), 562–569 (2021).
11. Li, X. & Jia, J. Research of the influences of the air flows on multiple scales on the transport and diffusion mechanisms of urban air pollution over the complex terrains. *Desert Oasis Meteorol.* **10** (6), 1–10 (2016).
12. Li, X. et al. Shallow Foehn on the Northern Leeside of Tianshan mountains and its influence on atmospheric boundary layer over urumqi, China—A Climatological study. *Atmos. Res.* **240**, 104940 (2020).
13. Li, X. et al. The role of Foehn in the formation of heavy air pollution events in urumqi, China. *J. Geophys. Res. Atmos.* **120** (11), 5371–5384 (2015).
14. Ayitikan, M. et al. Characteristics of Foehn wind in urumqi, china, and their relationship with EI Niño and extreme heat events in the last 15 years. *Climate.* **12** (4), 56 (2024).
15. Mamtimin, B. & Meixner, F. X. Air pollution and meteorological processes in the growing dryland City of Urumqi (Xinjiang, China). *Sci. Total Environ.* **409** (7), 1277–1290 (2011).
16. Al-Hemoud, A. et al. Temperature inversion and mixing height: critical indicators for air pollution in hot arid climate. *Nat. Hazards.* **97**, 139–155 (2019).
17. Wang, M. & Ming, H. Study on radar detection of one stratiform cloud precipitation process in the central part of the Tianshan mountains in China. *Asia-Pac. J. Atmos. Sci.* **54**, 511–524 (2018).
18. Liu, S., Triantis, K. & Zhang, L. The design of an urban roadside automatic sprinkling system: mitigation of PM2. 5–10 in ambient air in megacities. *Chin. J. Eng.* **2014** (1), 618109 (2014).
19. Wu, K. & Li, X. M. Deep learning for retrieving omni-directional ocean wave spectra from spaceborne synthetic aperture radar. *Remote Sens. Environ.* **314**, 114386 (2024).
20. Tan, X. et al. Modeling the water transport in water invasion channel with water invasion unit numerical simulation based on intelligent proxies. *Phys. Fluids*. **37**(2). (2025).
21. Yang, J. et al. Thermoacoustoelasticity for elastic wave propagation in preheated and prestressed solid rocks. *Rock Mech. Rock Eng.* 1–23 (2025).
22. Tan, X. H. et al. A fractal geometry-based model for stress-sensitive permeability in porous media with fluid-solid coupling. *Powder Technol.* 120774 (2025).
23. Feng, G. et al. Discussion on the weak equivalence principle for a Schwarzschild gravitational field based on the light-clock model. *Ann. Phys.* **473**, 169903 (2025).
24. Hou, Q. et al. Physics-informed neural network for diffusive wave model. *J. Hydrol.* **637**, 131261 (2024).
25. Peng, L., Liang, Y. & He, X. Transfers to Earth-Moon triangular libration points by Sun-perturbed dynamics. *Adv. Space Res.* **75** (3), 2837–2855 (2025).
26. Xu, X. et al. Three-dimensional reconstruction and geometric morphology analysis of lunar small craters within the patrol range of the Yutu-2 Rover. *Remote Sens.* **15** (17), 4251 (2023).

27. Sarkar, A. & De Ridder, K. The urban heat Island intensity of paris: a case study based on a simple urban surface parametrization. *Bound. Layer Meteorol.* **138**, 511–520 (2011).
28. Liu, L., Ran, L. & Sun, X. Analysis of the structure and propagation of a simulated squall line on 14 June 2009. *Adv. Atmos. Sci.* **32**, 1049–1062 (2015).
29. Srivastava, K. et al. Assimilation of Indian radar data with ADAS and 3DVAR techniques for simulation of a small-scale tropical cyclone using ARPS model. *Nat. Hazards.* **58**, 15–29 (2011).

Author contributions
All authors wrote the main manuscript text. All authors reviewed the manuscript.

Funding
Sponsored by the Natural Science Foundation of Xinjiang Uygur Autonomous Region (2024D01D33), the Science and Technology Program of the Xinjiang Production and Construction Corps (2023AB036), and the China Desert Meteorology Science Research Foundation (Sqj2022018).

Declarations

Competing interests
The authors declare no competing interests.

Additional information
Correspondence and requests for materials should be addressed to K.Z.

Reprints and permissions information is available at www.nature.com/reprints.

Publisher's note Springer Nature remains neutral with regard to jurisdictional claims in published maps and institutional affiliations.